

ULRR

New model for explaining the over-response phenomenon in percentage of depth dose curve measured using inorganic scintillating materials for optical fiber radiation sensors

Item Type	Article
Authors	Qin, Zhuang;Xie, Tianci;Dai, Xinyu;Zhang, Bin;Ma, Yu;Khan, Ihsan Ullah;Zhang, Xu;Li, Haopeng;Yan, Yongji;Zhao, Wenhui;Li, Song;Chen, Ziyin;Zhang, Daxin;Xu, Jun;Hu, Xiaokang;Xing, Lina;Feng, Kun;Lewis, Elfed;Sun, Weimin
Citation	Optics Express;27 (17)
Publisher	Optical Society of America
Download date	2026-03-16 05:34:07
Item License	https://creativecommons.org/licenses/by-nc-sa/1.0/
Link to Item	https://hdl.handle.net/10344/8526



New model for explaining the over-response phenomenon in percentage of depth dose curve measured using inorganic scintillating materials for optical fiber radiation sensors

ZHUANG QIN,¹ TIANCI XIE,¹ XINYU DAI,¹ BIN ZHANG,¹ YU MA,¹ IHSAN ULLAH KHAN,¹ XU ZHANG,¹ HAOPENG LI,¹ YONGJI YAN,¹ WENHUI ZHAO,¹ SONG LI,¹ ZIYIN CHEN,² DAXIN ZHANG,² JUN XU,³ XIAOKANG HU,³ LINA XING,³ KUN FENG,⁴ ELFED LEWIS,⁵ AND WEIMIN SUN^{1,*}

¹Key Lab of In-fiber Integrated Optics, Ministry Education of China, Harbin Engineering University, Harbin 150001, China

²Comprehensive Cancer Center, First Affiliated Hospital of Harbin Medical University, Harbin 150001, China

³Comprehensive Cancer Center, Second Affiliated Hospital of Harbin Medical University, Harbin 150001, China

⁴Shanghai Ninth People's Hospital, Shanghai 200011, China

⁵Optical Fibre Sensors Research Centre, University of Limerick, Castletroy, Limerick, Ireland

*sunweimin@hrbeu.edu.cn

Abstract: Inorganic scintillating material used in optical fibre sensors (OFS) when used as dosimeters for measuring percentage depth dose (PDD) characteristics have exhibited significant differences when compared to those measured using an ionization chamber (IC), which is the clinical gold standard for quality assurance (QA) assessments. The percentage difference between the two measurements is as high as 16.5% for a $10 \times 10 \text{ cm}^2$ field at 10 cm depth below the surface. Two reasons have been suggested for this: the presence of an energy effect and Cerenkov radiation. These two factors are analysed in detail and evaluated quantitatively. It is established that the influence of the energy effect is only a maximum of 2.5% difference for a beam size $10 \times 10 \text{ cm}^2$ compared with the measured ionization chamber values. And the influence of the Cerenkov radiation is less than 0.14% in an inorganic scintillating material in the case of OFS when using $\text{Gd}_2\text{O}_2\text{S:Tb}$ as the luminescent material. Therefore, there must be other mechanisms leading to over-response. The luminescence mechanism of inorganic scintillating material is theoretically analysed and a new model is proposed and validated that helps explain the over-response phenomenon.

© 2019 Optical Society of America under the terms of the [OSA Open Access Publishing Agreement](#)

1. Introduction

The ever-increasing sophistication of radiotherapy techniques, including those such as stereotactic radiosurgery, intensity-modulated radiation therapy, intraoperative radiation therapy, and intravascular brachytherapy, introduce new challenges to existing dosimetry systems. The most direct challenge is the need for a system that can provide real-time dose measurements with high spatial resolution, sensitivity and accuracy [1]. The absorbed dose is defined as the mean energy imparted by ionizing radiation to a mass in a finite volume [2]. The advantage of being able to identify small variations from the planned dose delivery at a very early stage of the treatment should be met using an *in-vivo* real-time sensor [3].

Many types of dosimeters have been investigated to measure absorbed radiation dose, including thermoluminescent dosimeters (TLDs), radiochromic films, metal-oxide semiconductor field effect transistors (MOSFETs), silicon diodes and ionization chambers (ICs) [4–8]. The TLDs and radiochromic films can provide high spatial resolution, but they

cannot provide real-time information as they need post irradiation processing and readout and calibration can be time consuming. ICs are a range of instruments that provide absolute radiation dose measurement, but the sizes of ICs generally mean that they cannot provide high spatial resolution and this combined with the fact that they rely on an electrical input for operation mean that they are unsuitable for *in-vivo* measurement. In addition, when used for quality assessment (QA) of clinical Linacs (linear accelerators), ICs should be used under water, but cannot be in direct contact with the water as this can potentially damage them. MOSFETs and silicon diodes can be used for real-time measurements, however, MOSFETs have a limited operating lifetime and they do not have sufficient sensitivity at distances beyond 10 cm from the radiation source. Silicon diodes are generally unstable over a prolonged period of usage and need employment of a number of correction factors, which requires additional care when applied to maintain accuracy. MOSFETs and Silicon diodes are also restricted to use on the patient's skin surface and therefore not adjacent to deep tissue tumors. In contrast, a new class of sensors using plastic optical fibers with embedded scintillators which possess the attractive characteristics of being small sized (can potentially be used in small field irradiation), are passive and can be hermetically sealed and further encapsulated in standard catheters (making them potentially useful truly *in-vivo*) and can measure in real time.

Optical fiber sensors (OFS) for radiation measurement can be classified according to the type of scintillator material used, namely organic and inorganic. Much attention has been focused on organic scintillator systems because these materials are highly tissue equivalent (through their small effective atomic number, Z_{eff}) which is important in terms of their interaction with irradiating electrons and X-rays, and feature dose linearity and good resistance to radiation damage [9–11]. However, organic scintillator systems have two clear shortcomings. The first is their low photon conversion efficiency and hence they provide generally low signal-noise ratios, and hence Cerenkov radiation emission can seriously influence their accuracy [12–14]. The second is the dependence of the generated signal on temperature [15–18]. However, inorganic scintillation systems also have some severe drawbacks including non-adherence to the curve of depth-dose and off-axis ratio which exhibit deviations with the calibrated quality assurance (QA) results measured using standard ICs [19]. They exhibit a clear over-response phenomenon which has been attributed to Cerenkov radiation and the high effective atomic (Z_{eff}) number which cause additional absorption (and hence emission) due to a combination of the Compton Scattering and the photoelectric effect, collectively referred to as an energy effect in this article [20].

In this paper, a study is conducted on the over-response phenomenon in the percentage depth dose curve measured using an inorganic scintillating material ($\text{Gd}_2\text{O}_2\text{S:Tb}$) in conjunction with radiation optical fiber sensor. A series of experiments and theoretical analysis is used to quantitatively assess the effects of photoelectric and Cerenkov radiation. Finally, a new physical model which explains the over-response phenomenon is proposed. The luminescence mechanism of the scintillating material is considered as the main reason for the over-response phenomenon, being separate from the Cerenkov radiation and the high Z number effect.

2. Methodology

The setup for measurement using the inorganic scintillation system for clinical (field) based measurements is shown in Fig. 1 and comprises the following:

1. The Linear accelerator (Linac). Three different types were used (Varian IX 3937, Elekta Synergy and an XHA 600D) which were used to produce high energy X rays (6MV) as experiments were conducted in three different hospitals.
2. The OFS which was used to detect the X-rays and produces fluorescence signals in the visible wavelength.

3. A Hamamatsu C11208-350 Multi Pixel photon counter (MPPC) and CH326 Photon counting detector (PCD) were used for monitoring the dynamic fluorescence intensity variations in real time. The MPPC detector was generally used in the early research phase, but owing to requirement of cost reduction for future commercial detection, the PCD was used in the later experiments.

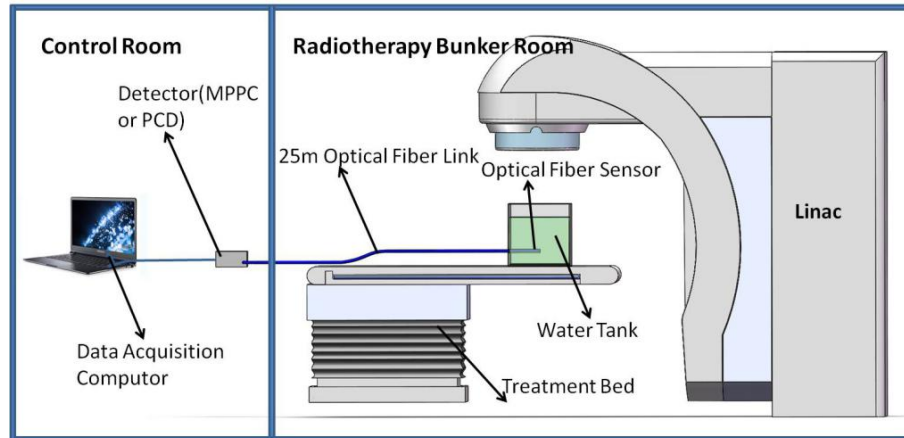


Fig. 1. Experimental setup.

As shown in Fig. 1, the OFS was placed inside a water phantom (used for QA in the clinic) at varying depths in the Radiotherapy Bunker Room. The Linac emits high energy X-rays when operating under standard conditions of a 100cm surface to source distance (SSD), a beam field size of $10 \times 10\text{cm}^2$ and a photon beam energy of 6 MVp. The OFS was constructed using a SH2001-J (ESKA) PMMA plastic optical fiber with an overall core and cladding diameter of $500 \mu\text{m}$ [21–23]. The structure of the dosimeter is shown schematically in Fig. 2. The core of the PMMA fiber was micro-machined to form a $200 \mu\text{m}$ diameter and 3 mm deep cavity at the tip of the fiber. An inorganic scintillating material $\text{Gd}_2\text{O}_2\text{S:Tb}$ (Phosphor Technology, UKL65/UF-R1), which fluoresces upon exposure to the incident ionizing radiation, was filled in the small hole and packaged in an epoxy mixture. When the sensor was exposed to linac's X-rays, the scintillating material emits a visible light signal which propagates along a 25m length of plastic optical fiber to the distal detector located in the control room. The OFS exhibited a strong signal response, a high S/N ratio, good repeatability, excellent dose linearity and isotropy with respect to the radial angular dependence as established in the previous article by the authors of this paper [21]. The repeatability of the OFS has been demonstrated and as the available testing time of the Linac in the clinical setting was limited, repeating results previously obtained was not considered appropriate for the investigation reported in this article.

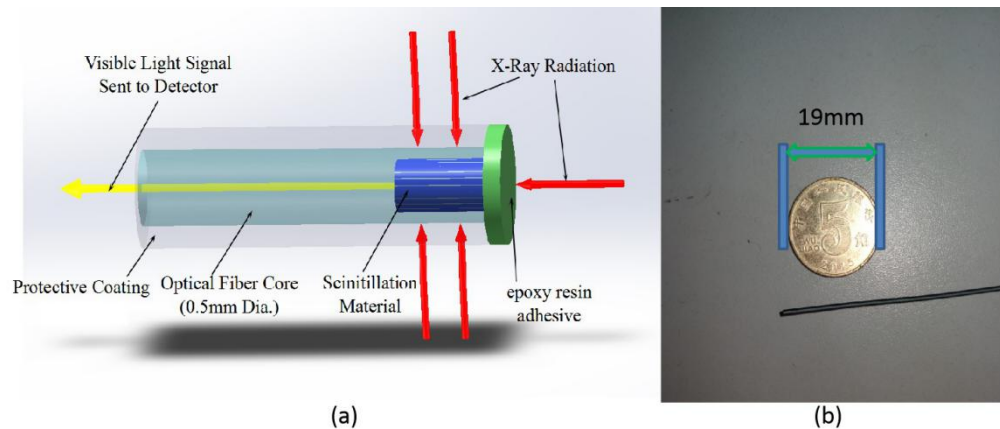


Fig. 2. The novel fiber-optic dosimeter. (a) Schematic representation and (b) the photograph.

3. Experimental result & discussion

The over-response is a well established phenomenon and has been previously reported by Alharbi et al in 2018 [20]. The classical over-response phenomenon is shown in Fig. 3. The figure shows the measured results using an ionization chamber (PTW30012) of dose versus depth below the surface of the water. These results were obtained at the clinic of First Affiliated Hospital of Harbin Medical University in Harbin. The figure also shows the simulation results obtained by Alharbi et al using a Monte Carlo (MC) method based on the software packages (BEAMnrc and DOSXYZnrc) [20,24,25]. Although the results of the MC simulations were of interest, they are limited by a lack of complexity of the model used. This is evident by the amount of deviation between the two sets of results. The figure also shows the OFS signal test by Qin et al in 2016 [21]. The response of the OFS (red dot points in Fig. 3) is much higher than the actual absorbed dose (blue solid line) at different depths in the water phantom.

3.1. Previous analysis of the over-response phenomenon

The over-response of the OFS is usually considered for two reasons. First, the over-response of the inorganic scintillating material with high effective atomic numbers, denoted with Z_{eff} , has been attributed to scattered radiation with low energy that is produced when the field sizes and/or the depth below the surface of the phantom increases [26–28]. But a comparison with the measured ionization chamber values with the MC simulation of the $\text{Gd}_2\text{O}_2\text{S:Tb}$ shows only maximum of 2.5% difference behind d_{max} for beam size $10 \times 10 \text{ cm}^2$ which is shown in Fig. 3 (black crosses). There is still a significant difference between the results obtained using the MC simulation and the experimentally captured results.

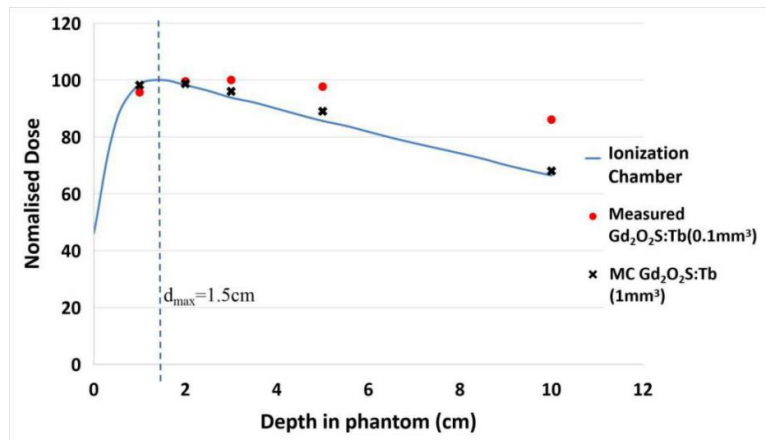


Fig. 3. Comparison of PDD profiles simulated using 1 mm³ Gd₂O₂S:Tb scintillating material (black crosses), measured using the OFS (blue dots) and measured using ionization chamber (solid red line) for field sizes 10 × 10 cm².

The second possible reason is the Cerenkov radiation contribution to the overall dose [20]. But the contribution of Cerenkov radiation depends on the percentage depth dose (PDD) curve of Cerenkov radiation and the relative intensity of Cerenkov radiation. The PDD curve for the 6 MVp photon beam obtained with Cerenkov radiation generated from a bare fiber (no scintillator included) by Jang et al is included in [29]. The PDDs obtained using an ionization chamber and simulated by MC are compared with those of the bare fiber. In Jang et al's work, the obtained PDD curves for the 6 MVp photon beam initially increased steeply with increasing depth, until reaching the depth for maximum dose (d_{max}), and then slowly decreased. The value of d_{max} obtained using the bare fiber, ionization chamber, and MC simulation was the same, being 1.5 cm for the 6 MVp photon beam. Dose differences between the results of the bare fiber and those of the ionization chamber and MC simulation were only about 0.6% and 0.7%, respectively. The PDD curve of the Cerenkov corrected radiation is very similar to the real absorbed dose curve. Therefore, the Cerenkov radiation provides only a very small contribution to the over-response phenomenon. In addition to the effect of the Cerenkov PDD curve, the intensity of the Cerenkov radiation relative to the signal intensity is also very important. In Martinez et al's work [26,27], the material YVO₄:Eu³⁺ was used as the inorganic scintillator which does not possess a relatively high luminous efficiency. The results of these investigations showed that it exhibits a 5.0% difference between the signals of a YVO₄:Eu³⁺ sensor with and without temporal subtraction of Cerenkov radiation when measuring the PDD profile for 3 × 3 cm² field at 10 cm depth [26,27]. Different scintillating materials have different luminous efficiency and therefore Fig. 3 could be dependent on the particular material selected. In the investigation of this work, another inorganic scintillating material, terbium-doped gadolinium oxysulfide (Gd₂O₂S:Tb) embedded in the OFS and a bare fiber were tested at the External Radiation Beam Therapy clinic of the First Affiliated Hospital of the Harbin Medical University, Harbin, China using a Varian IX 3937 Linac.

The OFS and a bare fiber were located centrally in the field of the ionizing beam which had a standard field size of 10 × 10 cm² at an SSD (Source to Surface Distance) of 100 cm. Both the OFS and the bare fiber were therefore exposed to near identical irradiation conditions for reference measurement and data validation. The OFS and the bare fiber were irradiated with a dose rate of 100 to 600MU/min with a photon energy of 6 MVp. The gate time of the MPPC detector was set to 100 ms and the photon detection threshold value for the MPPC set to its most sensitive setting, 0.5 (corresponding to single photon detection capability). The time resolved optical intensity received by the OFS and bare fiber is shown in

Fig. 4. Since the relative intensity of Cerenkov radiation can be considered very small as argued above, only the Cerenkov curve tested for a dose rate of 600MU/min (Monitory Units) is shown (the maximum value available). After calculation, it can be concluded that the accumulated intensity of Cerenkov is only 0.14% of the intensity measured by $Gd_2O_2S:Tb$. The intensity of the Cerenkov is less than the dark current background count value of the MPPC output and is therefore too small to effect the PDD curve of the $Gd_2O_2S:Tb$ embedded OFS.

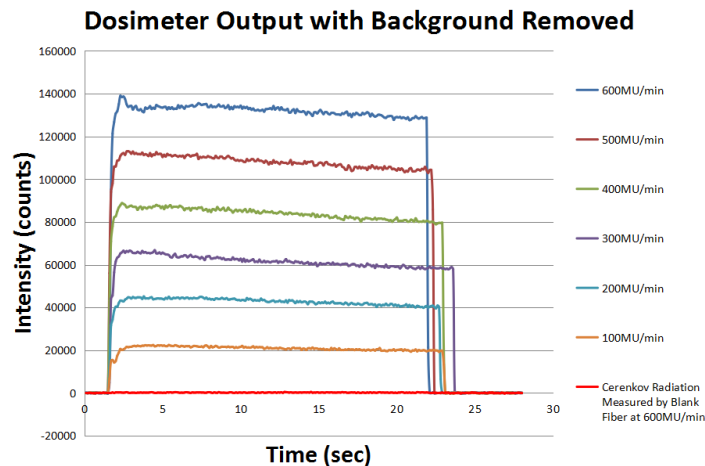


Fig. 4. The response of Cerenkov and OFS at different dose rate with background removed.

It is therefore likely that reasons other than the Z number and Cerenkov effects exist that result in the observed over-response phenomenon. The influence of different factors governing the absorbed dose and fluorescence of the scintillating material are discussed below.

3.2. The influence of high effective atomic numbers

Unlike some radiation dose sensors, including organic scintillation materials based sensors, with an effective Z number close to that of water, the incident photon energy on high Z_{eff} material based sensors has a profound effect on the measured dose value [30]. For beam energies in the single mega-voltage range, the Compton effect (whose cross section is nearly independent of the material's Z number) is the dominant effect. Therefore, it could be concluded that there is no difference between high Z_{eff} sensors and water equivalent sensors in this energy range.

- (i) Multiple Compton scattering can occur, leading to the generation of lower energy photons which can ultimately result in a photoelectric effect occurring within the material when the photon energy has reached below 1 MVp. Also, due to the presence of this type of scattering, the percentage of lower energy photons increases with the dimension of the beam size and increasing water depth [31–34].
- (ii) There is also a contribution from a 'direct' photoelectric effect from the beam. In all cases of clinical linacs, the peak of the beam energy may be in the MV range (e.g. in the case of this investigation 6 MVp), but the beam profile with energy means that a significant section of the beam's energy profile populates values as low as the kV range [31–34]. As the photoelectric effect dominates in the case of relatively high Z number (Z^4) material when the beam energy is in the kV range, the scintillating material with its relatively high Z number has a larger cross section than water. Therefore, additional electrons are created in the scintillating material. Some recent papers have reported that this directly leads to an over-response of dose deposition [20,27]. However, the position in the tissue

phantom (water in the case of this investigation) where the X ray loses its energy is not necessarily the position at which the energy is deposited. In a given volume, the real absorbed dose is equivalent to the energy lost by the secondary electrons ionizing or exciting the medium minus the energy lost by the secondary electrons producing bremsstrahlung radiation. The key point is the loss due to the secondary electrons, not the loss due to the X ray that reacts with the medium, and specifically electronic equilibrium [35,36] does not exist within the scintillating material. Most of the secondary electrons that excite the scintillating material are actually produced in the water as shown schematically in Fig. 5. Most of the energy of the electrons produced in the scintillating material is deposited in a deeper position than the OFS. Therefore, the over response of the dose deposition due to the high Z number is relatively small as suggested in the simulation result in Fig. 3.

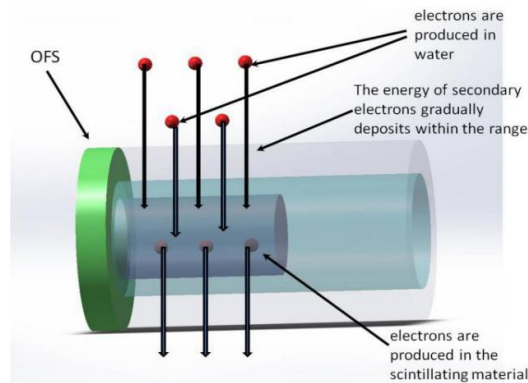


Fig. 5. Schematic diagram of deposition of secondary electrons in OFS.

3.3. Effect of Cerenkov radiation on PDD curve formation

Cerenkov radiation is produced directly by interactions between charged particles and a medium, and the intensity of the Cerenkov radiation is proportional to the volume of the irradiated medium in general. When the volume of the irradiated medium and the irradiation angle is fixed, the PDD curve of Cerenkov should be similar with that measured by the IC. However, there exists some differences between these two curves. The charged particles should have enough energy to produce Cerenkov radiation. The Cerenkov threshold energy (CTE; E_{th}) of the charged particles can be calculated using the special theory of relativity [37]:

$$E_{th} = m_0 c^2 \left(\frac{n}{\sqrt{n^2 - 1}} - 1 \right) \quad (1)$$

where m_0 is the rest mass of the charged particle, c is the velocity of light in vacuum, and n is the refractive index of the host medium. The CTE of an electron to produce Cerenkov radiation in PMMA is 178 keV [29]. At a near-surface depth, since the therapeutic photon beam generated from the Linac consists of bremsstrahlung photons, there exist low-energy photons (below 178 keV) in the energy spectrum of the generated photon beam. Photons in this energy range are rapidly attenuated at depths of several millimeters in the water [38]. Therefore, the ratios of electron fluxes which can produce Cerenkov radiation to total electron fluxes which cause dose deposition become lower at a deeper depth. In this condition, there exists a larger proportion of low-energy electrons which cannot generate Cerenkov radiation in the near-surface region. Therefore, small dose differences exist in the depth dose characteristic for the photon beam. In Jang *et al.*'s work, the near-surface depth was calculated to be less than 0.86 mm using MC simulation [29]. But this difference is quite small as shown

by Jang *et al* [29]. When the intensity of the Cerenkov radiation is only 0.14% of the fluorescence intensity, the Cerenkov clearly has little or no impact on the PDD curve.

3.4. New physical model explains the over-response phenomenon

The percentage difference between the over-response curve and real PDD curve of Fig. 3 is 16.5% for a $10 \times 10 \text{ cm}^2$ field at 10 cm depth. But the effects of the photoelectric effect and the Cerenkov radiation are less than 3%. Therefore a new physical model to explain the over-response is proposed in this article. The principle which determines the capability of scintillating materials to detect incoming ionizing radiation via fluorescence can be complicated, and is outlined as follows:

- (i) When scintillating materials are irradiated using X-rays, γ rays or other high-energy particles, the valence electrons enter the excited state due to excitation, that is, electrons transfer from the valence band to the conduction band. When the electrons spontaneously transfer back from the conduction band to the valence band, fluorescence can be caused by both energetic electrons and X-ray photons. However, only electronic excitation is considered in the case of the dose deposition process, and X-ray photon excitation is not reflected in the dose deposition process. The scintillating material has a broad excitation spectrum in the low energy region. The fluorescence effect causes the material to absorb X-ray and ultraviolet light to emit visible light which is detected at the distal end of the optical fiber using a photodetector e.g. MPPC. The fact that the scintillating material absorbs X-rays can be proved on the basis of a simple experiment that was conducted by the authors of this paper at the Shanghai Ninth People's Hospital of China. A $\text{Gd}_2\text{O}_2\text{S:Tb}$ embedded OFS was located on the central axis and at a source-target distance (STD) of 101.5cm under different conditions described herein. The sensor was irradiated by the X-ray beam of a Linac with energy 6MV, to deliver a dose 200MU in two separate tests using an Elekta Synergy Linac. The only difference between the two tests was the medium in which the OFS was located. In one experiment the OFS was located on the Linac patient bed and therefore was in an air (free space). In the other test the OFS was located at a depth of 1.5cm (d_{max}) in a water phantom. The intensity measured using the MPPC when testing was 4.47×10^7 counts in water and 2.72×10^7 counts in air. The intensity in air is therefore 60.7% of the value measured in water. The density of air is only 1/775 of water, and therefore the amount of secondary electron flux produced in air is clearly very small compared to that in water. This shows that the OFS interacts directly with X-ray photons in a large proportion of both modes of action (interacts with X-ray photons and electrons). However, it is not possible that this part of visible light signal caused by X-Ray photons reflects the energy deposition at this position. Since electronic equilibrium is not satisfied, and most of the electrons being generated by the Compton and photoelectric effect at this position are deposited at a deeper depth (the thickness of scintillating material is $200\mu\text{m}$ in diameter within the OFS probe) when the scintillating material is excited as discussed in Section 3.2. On the other hand, the intensity of the visible light caused by X-ray photons is closely related to the energy of incoming X-rays. An energy dependence experiment was also conducted at the Shanghai Ninth People's Hospital of China. An OFS comprising $\text{Gd}_2\text{O}_2\text{S:Tb}$ was located on the central axis and at a STD (source-tumor distance) of 100cm in air. The sensor was irradiated for a 200MU dose using two separate Linac delivered X-ray beams of 6MVp and 10MVp energies from an Elekta Synergy Linac. The result is shown in Fig. 6. It shows that the scintillating material has a stronger response to the lower energy photons in the megavolt range. However, this conclusion requires further experimental investigation (using different X-ray energies). A stronger over-response at deeper positions could be expected as predicted in Fig. 3, because the scattered X-ray energy is lower at the deeper positions and the scintillator material responds more strongly.

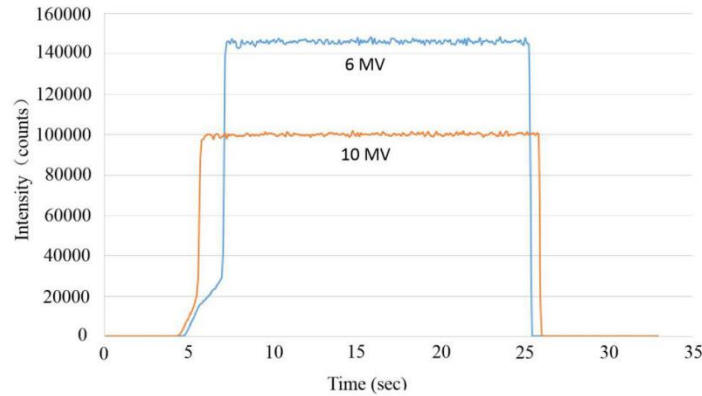


Fig. 6. The energy dependence of the response of the $\text{Gd}_2\text{O}_2\text{S:Tb}$ sensor.

- (ii) The orbital electron energy of scintillating materials is relatively high, and it is divided into many states by its crystal field and spin. When secondary electrons of different energies interact with the scintillating material, e.g. $\text{Gd}_2\text{O}_2\text{S:Tb}$, these fluorescent molecules are excited to different excited energy states. This excitation energy is the energy deposition of radiation in the scintillating material. Through the process of vibrational relaxation and internal conversion, the de-excited electronic states mainly transition to the $^5\text{D}_4$ state. Following the process of vibrational relaxation and internal conversion, the electrons de-excite from $^5\text{D}_4$ excited state level to $^7\text{F}_j$ ($j = 0-6$) ground state levels and visible fluorescence light is emitted. The peak at 544 nm according to the $^5\text{D}_4 \rightarrow ^7\text{F}_5$ transition is the strongest [39]. The energy of the visible light signal does not represent the deposition dose and this part of energy is relatively constant, affected only by doping concentration and temperature [40]. Unlike luminescence energy, because the electrons are in different excited states, electrons have different excitation energies which represent the deposition dose. Therefore, the ratio of light energy and excitation energy is variable. When the energy of the secondary electron is low, the ratio is definitely large. In some experiments (e.g. depth, beam size, etc.), electrons at different locations have different energies, the change of the ratio has a clear impact on the measurements. In the case of the depth dose experiment, as the depth increases, the X ray energy spectrum shifts to lower energies, and more low-energy electrons are produced. When these electrons of lower energy are absorbed by the scintillating material, more visible light signals are generated because the ratio becomes larger. Thus, as the depth increases, the PDD curve of the scintillating material produces a greater over-response signal. Correspondingly, if the beam size is changed, the photon energy spectrum varies at the same depth on the central axis. So the PDD curves for different beam size are also affected, which has been experimentally verified and described later in this article (Section 3.5).
- (iii) Inorganic scintillation materials generally have a relatively high effective atomic number, e.g. $\text{Gd}_2\text{O}_2\text{S:Tb}$, has a Z_{eff} of 59.4. This clearly results in a stronger bremsstrahlung which can be deduced using quantum electrodynamic theory [2]:

$$\left(\frac{S}{\rho}\right)_{\text{rad}} \propto \frac{z^2 Z^2}{m^2} NE \quad (2)$$

where $\left(\frac{S}{\rho}\right)_{\text{rad}}$ is the mass radiative stopping power that represents the bremsstrahlung loss of charged particles, z is the charge number of charged particles, Z is the atomic

number of the target atom, N is number of atoms in unit mass target material, m is static mass of charged particles, E is the energy of charged particles. These extra X-ray photons have the effect of producing additional fluorescence that will definitely change the PDD curve even if the light intensity is not very large. But the mass radiative stopping power is proportional to the energy of the charged particles. That means this part of the over-response is smaller at larger depths or if the beam size is larger. However, the real PDD curve (as measured using a standard IC) exhibits exactly the opposite trend. Therefore, it can be concluded that the effect of bremsstrahlung must also be relatively small and could be ignored.

3.5. Verification of analysis

As the new model shows, if low-energy photons and electrons generate additional visible light signals, the application of the scintillating material sensor is influenced under different conditions. For example, if the beam size is larger, more low-energy scattered photons are produced, then the over-response phenomenon becomes more pronounced. This conclusion can also be proved by experiment. An OFS was tested at the Second Affiliated Hospital of Harbin Medical University of China for its response to a 100 MU dose at an X-ray photon energy of 6 MVp with field size values of $3 \times 3 \text{ cm}^2$, $4 \times 4 \text{ cm}^2$, $5 \times 5 \text{ cm}^2$, $6 \times 6 \text{ cm}^2$, $8 \times 8 \text{ cm}^2$, $10 \times 10 \text{ cm}^2$, $12 \times 12 \text{ cm}^2$, $15 \times 15 \text{ cm}^2$, $20 \times 20 \text{ cm}^2$, $25 \times 25 \text{ cm}^2$ using an XHA600D Linac. It is clear from the result in Fig. 7 that the over-response of the OFS becomes greatly pronounced with increasing field size. Meanwhile the peaks of the curves shift to a deeper position. Another example is the effect on the dosimetric penumbra shown in Fig. 8. The physical penumbra width is defined as the distance between 20% and 80% of the iso-dose curves at a reference depth and it is the sum of geometrical, transmission and radiological penumbra [41]. The penumbra of the OFS is much wider than that of the IC. This is due to the fact that there are more low-energy scattered photons at the edge of the field [42]. But when the OFS probe is covered using a Sn (1mm thick) shield (to block the low-energy rays), the penumbra is reduced from 4.5cm to 0.6cm. The apparent reduction in intensity outside the beam field once again proves that the $\text{Gd}_2\text{O}_2\text{S:Tb}$ embedded OFS has a stronger response to low energy particles. It also proves that it is possible to correct for the over-response by shielding to avoid the creation of low energy photons. In addition to the shielding method, a two-different-inorganic-scintillating-materials method was formulated to calibrate the over-response phenomenon in a previous article by some of the authors of this article [43].

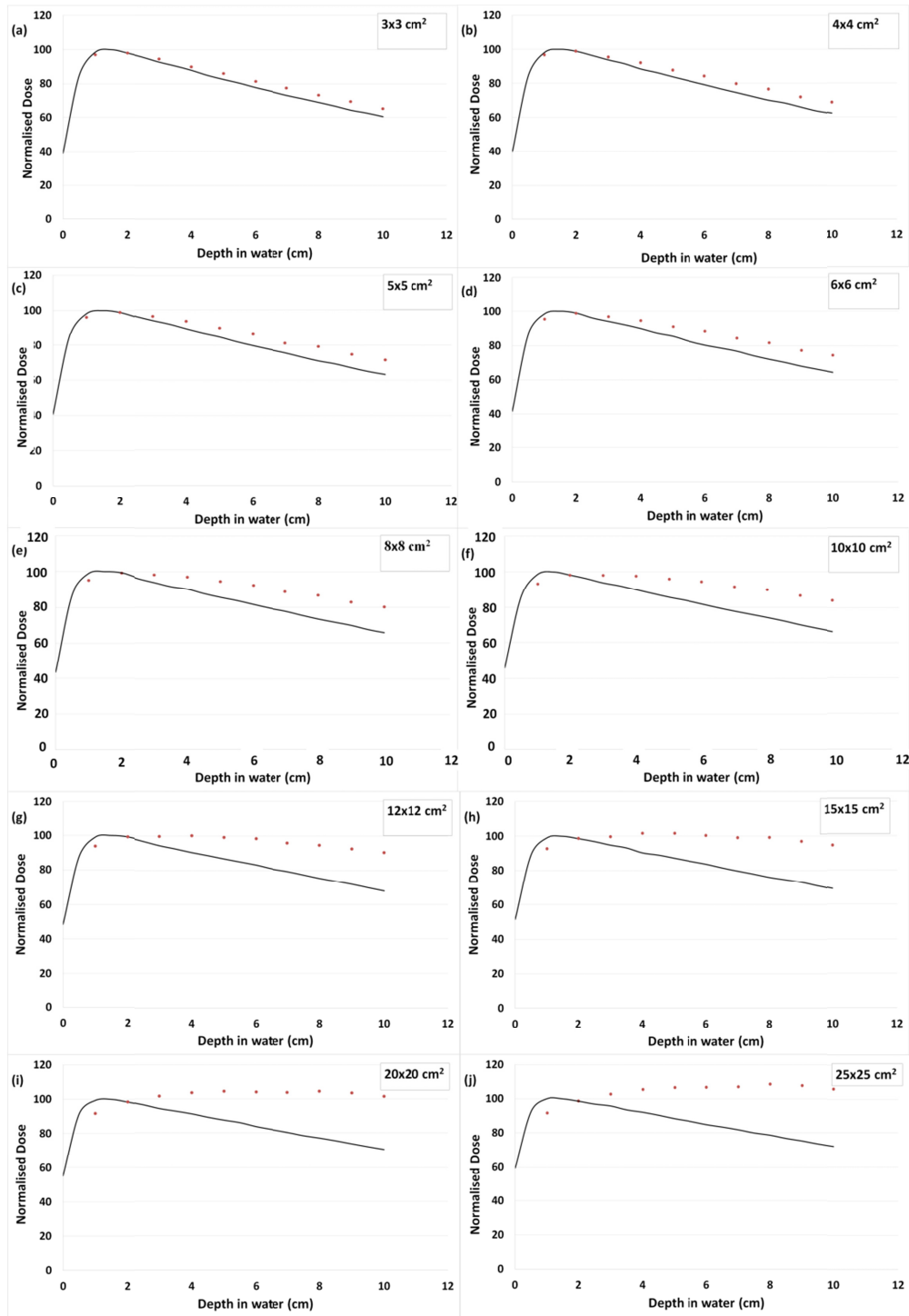


Fig. 7. PDD measurements obtained using the OFS (orange dots) compared to ionization chamber measurements (solid line). The difference between the two curves increases with the increase in field sizes. (a) $3 \times 3 \text{ cm}^2$. (b) $4 \times 4 \text{ cm}^2$. (c) $5 \times 5 \text{ cm}^2$. (d) $6 \times 6 \text{ cm}^2$. (e) $8 \times 8 \text{ cm}^2$. (f) $10 \times 10 \text{ cm}^2$. (g) $12 \times 12 \text{ cm}^2$. (h) $15 \times 15 \text{ cm}^2$. (i) $20 \times 20 \text{ cm}^2$ and (j) $25 \times 25 \text{ cm}^2$, respectively.

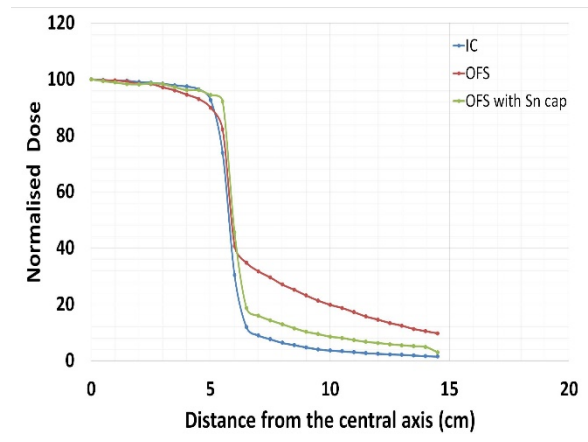


Fig. 8. Off-axis ratio (OAR) curve tested by IC, OFS and OFS with Sn cap.

4. Conclusion

The over-response phenomenon of a measured PDD curve obtained using an optical fibre sensor with an inorganic scintillator material ($\text{Gd}_2\text{O}_2\text{S:Tb}$) as a dosimeter has been discussed. The over-response phenomenon has previously been attributed to the influence of the photoelectric effect caused by the high equivalent atomic number and the Cerenkov radiation received by the fiber optic sensor. However, the maximum difference in d_{max} accounts for only 2.5% for a beam size $10 \times 10 \text{ cm}^2$ and is principally caused by the photoelectric effect compared with the measured ionization chamber values with the a separately conducted MC simulation of the $\text{Gd}_2\text{O}_2\text{S:Tb}$ based sensor.

Through theoretical analysis, it can be argued that the extra secondary electrons due to the photoelectric effect are not completely deposited in the OFS as the effect due to the photoelectric effect is very small. On the other hand, the PDD curve of the Cerenkov radiation is basically consistent with the actual PDD curve measured using a standard IC, and only leads to an under-response at depth values less than 0.86 mm where the effect is very small. The intensity of the Cerenkov is only 0.14% of the intensity measured using $\text{Gd}_2\text{O}_2\text{S:Tb}$. Furthermore, a theoretical analysis of the Cerenkov radiation has shown that it is extremely unlikely that Cerenkov radiation accounts for any over-response.

In this paper, a new model that can explain the over-response phenomenon has been proposed based on: (i) Both energetic photons and electrons being the cause of the fluorescence. Among them, a significant energy dependence on photon response has been found. The scintillating material has a stronger response to the lower energy photons. (ii) For the absorption of electron energy, different energy absorption events may emit the same intensity of light. These two points lead to a stronger response to low-energy photons and electrons. Eventually they lead to an over-response phenomenon which is observable in the PDD curve. This theory was proved by shielding the low energy particles and different beam size experiments. Through a theoretical analysis and experimental verification, the PDD over-response phenomenon can be corrected in part by shielding or using two-different-inorganic-scintillating-materials simultaneously. However, shielding using a shield cap is not suitable for clinical use, and the use of an alternative method for calibration is necessary. Further investigations using alternative scintillator materials (other than $\text{Gd}_2\text{O}_2\text{S:Tb}$) are also ongoing.

Funding

Natural Science Foundation of Heilongjiang Province (ZD2019H003); Joint Research Fund in Astronomy (U1631239, U1331114) under cooperative agreement between the National Natural Science Foundation of China (NSFC) and Chinese Academy of Sciences (CAS);

International Science & Technology Cooperation Program of China (2014DFE10030); 111 Project (B13015); Fundamental Research Funds for the Central Universities to the Harbin Engineering University.

References

1. B. Mijnheer, S. Beddar, J. Izewska, and C. Reft, "In vivo dosimetry in external beam radiotherapy," *Med. Phys.* **40**(7), 070903 (2013).
2. E. B. Podgorsak, *Radiation Oncology Physics: A Handbook for Teachers and Students* (International Atomic Energy Agency, 2005), Chap. 2.
3. J. Shafiq, M. Barton, D. Noble, C. Lemer, and L. J. Donaldson, "An international review of patient safety measures in radiotherapy practice," *Radiother. Oncol.* **92**(1), 15–21 (2009).
4. J. Lambert, T. Nakano, S. Law, J. Elsey, D. R. McKenzie, and N. Suchowerska, "In vivo dosimeters for HDR brachytherapy: A comparison of a diamond detector, MOSFET, TLD, and scintillation detector," *Med. Phys.* **34**(5), 1759–1765 (2007).
5. C. R. Edwards, S. Green, J. E. Palethorpe, and P. J. Mountford, "The response of a MOSFET, p-type semiconductor and LiF TLD to quasi-monoenergetic x-rays," *Phys. Med. Biol.* **42**(12), 2383–2391 (1997).
6. D. Manigandan, G. Bharanidharan, P. Aruna, K. Devan, D. Elangovan, V. Patil, R. Tamilarasan, S. Vasanthan, and S. Ganesan, "Dosimetric characteristics of a MOSFET dosimeter for clinical electron beams," *Phys. Med.* **25**(3), 141–147 (2009).
7. D. E. Hyer, R. F. Fisher, and D. E. Hintenlang, "Characterization of a water-equivalent fiber-optic coupled dosimeter for use in diagnostic radiology," *Med. Phys.* **36**(5), 1711–1716 (2009).
8. L. A. Benevides, A. L. Huston, B. L. Justus, P. Falkenstein, L. F. Brateman, and D. E. Hintenlang, "Characterization of a fiber-optic-coupled radioluminescent detector for application in the mammography energy range," *Med. Phys.* **34**, 2220–2227 (2007).
9. A. S. Beddar, T. R. Mackie, and F. H. Attix, "Water-equivalent plastic scintillation detectors for high-energy beam dosimetry: I. Physical characteristics and theoretical consideration," *Phys. Med. Biol.* **37**(10), 1883–1900 (1992).
10. A. S. Beddar, T. R. Mackie, and F. H. Attix, "Water-equivalent plastic scintillation detectors for high-energy beam dosimetry: II. Properties and measurements," *Phys. Med. Biol.* **37**(10), 1901–1913 (1992).
11. D. Flüh, M. Heintz, F. Indenkampen, C. Wiczorek, H. Kolanoski, and U. Quast, "Direct reading measurement of absorbed dose with plastic scintillators--the general concept and applications to ophthalmic plaque dosimetry," *Med. Phys.* **23**(3), 427–434 (1996).
12. A. S. Beddar, T. J. Kinsella, A. Ikhlef, and C. H. Sibata, "A miniature 'scintillator-fiber-optic-PMT' detector system for the dosimetry of small fields in stereotactic radiosurgery," *IEEE Trans. Nucl. Sci.* **48**(3), 924–928 (2001).
13. M. A. Clift, R. A. Sutton, and D. V. Webb, "Dealing with Cerenkov radiation generated in organic scintillator dosimeters by bremsstrahlung beams," *Phys. Med. Biol.* **45**(5), 1165–1182 (2000).
14. A. S. Beddar, "Plastic scintillation dosimetry and its application to radiotherapy," *Radiat. Meas.* **41**, S124–S133 (2006).
15. S. Beddar, "On possible temperature dependence of plastic scintillator response," *Med. Phys.* **39**(10), 6522 (2012).
16. S. Buranurak, C. E. Andersen, A. R. Beierholm, and L. R. Lindvold, "Temperature variations as a source of uncertainty in medical fiber-coupled organic plastic scintillator dosimetry," *Radiat. Meas.* **56**, 307–311 (2013).
17. J. A. Tanyi, S. P. Krafft, T. Ushino, A. L. Huston, and B. L. Justus, "Performance characteristics of a gated fiber-optic-coupled dosimeter in high-energy pulsed photon radiation dosimetry," *Appl. Radiat. Isot.* **68**(2), 364–369 (2010).
18. L. Wootton and S. Beddar, "Temperature dependence of BCF plastic scintillation detectors," *Phys. Med. Biol.* **58**(9), 2955–2967 (2013).
19. J. Y. Huang, D. S. Followill, X. A. Wang, and S. F. Kry, "Accuracy and sources of error of out-of field dose calculations by a commercial treatment planning system for intensity-modulated radiation therapy treatments," *J. Appl. Clin. Med. Phys.* **14**(2), 4139 (2013).
20. M. Alharbi, M. Martyn, L. X. Chen, S. Gillespie, P. Woulfe, S. O'Keefe, and M. Foley, "Novel optical fibre sensors and their applications in radiotherapy," *Proc. SPIE* **10680**, 106800Z (2018).
21. Q. Zhuang, H. Yaosheng, M. Yu, Z. Wenhui, S. Weimin, Z. Daxin, C. Ziyin, and L. Elfed, "Embedded structure fiber-optic radiation dosimeter for radiotherapy applications," *Opt. Express* **24**(5), 5172–5185 (2016).
22. S. O'Keefe, W. H. Zhao, W. M. Sun, D. X. Zhang, Z. Qin, Z. Y. Chen, Y. Ma, and E. Lewis, "An optical fibre-based sensor for real-time monitoring of clinical linear accelerator radiotherapy delivery," *IEEE J. Sel. Top. Quant.* **22**(3), 5600108 (2016).
23. C. Penner, C. Hoehr, S. O'Keefe, P. Woulfe, and C. Duzenli, "Characterization of a Terbium-activated Gadolinium Oxysulfide plastic optical fiber sensor in photons and protons," *IEEE Sens. J.* **18**(4), 1513–1519 (2018).
24. D. W. O. Rogers, B. Walters, and I. Kawrakow, *BEAMnrc Users Manual* (National Research Council of Canada, 2013).

25. B. Walters, I. Kawrakow, and D. W. O. Rogers, *DOSXYZnrc Users Manual* (National Research Council of Canada, 2005).
26. N. Martínez, A. Rucci, J. Marcazzó, P. Molina, M. Santiago, and W. Cravero, "Characterization of $\text{YVO}_4:\text{Eu}^{3+}$ scintillator as detector for Fiber Optic Dosimetry," *Radiat. Meas.* **106**, 650–656 (2017).
27. N. Martínez, T. Teichmann, P. Molina, M. Sommer, M. Santiago, J. Henniger, and E. Caselli, "Scintillation properties of the $\text{YVO}_4:\text{Eu}^{3+}$ compound in powder form: its application to dosimetry in radiation fields produced by pulsed mega-voltage photon beams," *Z. Med. Phys.* **25**(4), 368–374 (2015).
28. M. Ramírez, N. Martínez, J. Marcazzó, P. Molina, D. Feld, and M. Santiago, "Performance of $\text{ZnSe}(\text{Te})$ as fiberoptic dosimetry detector," *Appl. Radiat. Isot.* **116**, 1–7 (2016).
29. K. W. Jang, T. Yagi, C. H. Pyeon, W. J. Yoo, S. H. Shin, C. Jeong, B. J. Min, D. Shin, T. Misawa, and B. Lee, "Application of Cerenkov radiation generated in plastic optical fibers for therapeutic photon beam dosimetry," *J. Biomed. Opt.* **18**(2), 027001 (2013).
30. J. Wuerfel, "Dose measurements in small fields," *Med. Phys. Internat.* **1**(1), 81–90 (2013).
31. C. R. Edwards and P. J. Mountford, "Near surface photon energy spectra outside a 6 MV field edge," *Phys. Med. Biol.* **49**(18), N293–N301 (2004).
32. G. X. Ding, "Energy spectra, angular spread, fluence profiles and dose distributions of 6 and 18 MV photon beams: results of monte carlo simulations for a varian 2100EX accelerator," *Phys. Med. Biol.* **47**(7), 1025–1046 (2002).
33. M. S. Teixeira, D. V. S. Batista, D. Braz, and L. A. R. da Rosa, "Monte Carlo simulation of Novalis Classic 6 MV accelerator using phase space generation in GATE/Geant4 code," *Prog. Nucl. Energy* **110**, 142–147 (2019).
34. A. Skrobala, S. Adameczyk, M. Kruszyna-Mochalska, M. Skórska, A. Konefał, W. Suchorska, K. Zaleska, A. Kowalik, W. Jackowiak, and J. Malicki, "Low dose out-of-field radiotherapy, part 2: Calculating the mean photon energy values for the out-of-field photon energy spectrum from scattered radiation using Monte Carlo methods," *Cancer Radiother.* **21**(5), 352–357 (2017).
35. J. Dutreix, A. Dutreix, and M. Tubiana, "Electronic Equilibrium and Transition Stages," *Phys. Med. Biol.* **10**(2), 177–190 (1965).
36. J. R. Greening, *Fundamentals of Radiation Dosimetry* (CRC Press, 2017).
37. Z. W. Bell and L. A. Boatner, "Neutron detection via the Cherenkov effect," *IEEE Trans. Nucl. Sci.* **57**(6), 3800–3806 (2010).
38. W. R. Hendee, G. S. Ibbott, and E. G. Hendee, *Radiation Therapy Physics* (New York, 2005).
39. E. I. Gorokhova, V. A. Demidenko, S. B. Mikhlin, P. A. Rodnyi, and C. W. E. van Eijk, "Luminescence and scintillation properties of $\text{Gd}_2\text{O}_3:\text{Tb}$, Ce ceramics," *IEEE Trans. Nucl. Sci.* **52**(6), 862827 (2005).
40. Z. H. Xu, Y. X. Li, Z. F. Liu, and D. Wang, "UV and X-ray excited luminescence of Tb^{3+} -doped ZnGa_2O_4 phosphors," *J. Alloys Compd.* **391**(1-2), 202–205 (2005).
41. A. Mahmoudi, G. Geraily, A. Shirazi, and T. H. Nia, "Penumbra reduction technique and factors affecting it in radiotherapy machines – Review study," *Radiat. Phys. Chem.* **157**, 22–27 (2019).
42. C. R. Edwards and P. J. Mountford, "Near surface photon energy spectra outside a 6 MV field edge," *Phys. Med. Biol.* **49**(18), N293–N301 (2004).
43. Z. Qin, Y. Hu, Y. Ma, W. Lin, X. Luo, W. Zhao, W. Sun, D. Zhang, Z. Chen, B. Wang, and E. Lewis, "Water-equivalent fiber radiation dosimeter with two scintillating materials," *Biomed. Opt. Express* **7**(12), 4919–4927 (2016).